

Dependence of the critical temperature in overdoped copper oxides on superfluid density

I. Božović^{1,2}, X. He^{1,2}, J. Wu¹ & A. T. Bollinger¹

The physics of underdoped copper oxide superconductors, including the pseudogap, spin and charge ordering and their relation to superconductivity^{1–3}, is intensely debated. The overdoped copper oxides are perceived as simpler, with strongly correlated fermion physics evolving smoothly into the conventional Bardeen–Cooper–Schrieffer behaviour. Pioneering studies on a few overdoped samples^{4–11} indicated that the superfluid density was much lower than expected, but this was attributed to pair-breaking, disorder and phase separation. Here we report the way in which the magnetic penetration depth and the phase stiffness depend on temperature and doping by investigating the entire overdoped side of the $\text{La}_{2-x}\text{Sr}_x\text{CuO}_4$ phase diagram. We measured the absolute values of the magnetic penetration depth and the phase stiffness to an accuracy of one per cent in thousands of samples; the large statistics reveal clear trends and intrinsic properties. The films are homogeneous; variations in the critical superconducting temperature within a film are very small (less than one kelvin). At every level of doping the phase stiffness decreases linearly with temperature. The dependence of the zero-temperature phase stiffness on the critical superconducting temperature is generally linear, but with an offset; however, close to the origin this dependence becomes parabolic. This scaling law is incompatible with the standard Bardeen–Cooper–Schrieffer description.

Using atomic-layer-by-layer molecular beam epitaxy (ALL-MBE; refs 12, 13), we synthesized single-crystal films of $\text{La}_{2-x}\text{Sr}_x\text{CuO}_4$ (LSCO), the simplest copper oxide that we can dope all the way to a non-superconducting metal state. As single-layer LSCO sustains high-temperature superconductivity (HTS) with a T_c value as high as is found in bulk samples¹³, the physics is quasi-two-dimensional (2D) and we focus on the in-plane properties.

We used the mutual inductance technique^{9,10,14–16} (Fig. 1a–c and Extended Data Figs 1 and 2), improved (see Methods) to resolve the absolute value of λ with a $\pm 1\%$ accuracy. For this, it is critical to accurately determine the superconducting layer thickness, which we achieve by engineering the samples at the atomic-layer level as illustrated in Fig. 1d. The sharpness of the peak in $\text{Im}V_p(T)$, or equivalently in $\text{Im}M(T)$, where V_p is the voltage on the pick-up coil and M is the mutual inductance, puts an upper bound of about 0.1 K on the spread in T_c (defined by the onset of the Meissner effect, that is, the expulsion of the magnetic field) in this $10 \times 10 \text{ mm}^2$ film.

We have studied over 2,000 LSCO films in great detail (see Extended Data Figs 3–7). The film thickness was varied from $d = 0.66 \text{ nm}$ (half of the unit cell height) to over 100 nm, and the composition was varied across the entire phase diagram. This was crucial for obtaining definitive conclusions—copper oxides are complex compounds, HTS has largely been a materials science endeavour, and good statistics are essential.

In Fig. 2 we show our key experimental data extracted directly from the measured inductance with dense coverage of the entire overdoped LSCO region. Figure 2a shows the doping dependence of $\lambda(T)$ for the hundred most homogeneous films, which are likely to represent the intrinsic LSCO properties. Figure 2b, c shows the 2D superfluid

phase stiffness $\rho_s \equiv A/\lambda^2$, which is directly proportional to the 2D superfluid density $n_s^{2D} = \rho_s(4k_B m^*/\hbar^2)$. Here $A = \hbar^2 d/4\mu_0 k_B e^2 = 3.55 \times 10^{-12} \text{ m}^2 \text{ K}^{-1}$, k_B is the Boltzmann constant, m^* is the electron effective mass, \hbar is the reduced Planck constant, $\mu_0 = 4\pi \times 10^{-7} \text{ N A}^{-2}$ is the vacuum permeability and e is the electron charge. The $\rho_s(T)$ dependence is essentially linear, even in the heavily overdoped LSCO films (Fig. 2c). A crossover to a T^2 -dependence occurs below a very low sample-dependent temperature T^{**} . Figure 2d shows the dependence of T_c on ρ_{s0} . (The subscript 0 refers to the $T \rightarrow 0$ limit; this extrapolation is justified because our measurements extend down to $T = 300 \text{ mK}$.) The $T_c(\rho_{s0})$ scaling in Fig. 2d is largely linear, $T_c = T_0 + \alpha\rho_{s0}$, with $T_0 = (7.0 \pm 0.1) \text{ K}$ and the proportionality coefficient $\alpha = 0.37 \pm 0.02$, except very close to the origin where the curve fits closely to $T_c = \gamma\sqrt{\rho_{s0}}$, where $\gamma = (4.2 \pm 0.5) \text{ K}^{1/2}$. The data are as accurate as depicted in the figure; the error bars are smaller than the marker size.

Our findings reinforce pioneering observations^{4–7} of the diminishing ρ_{s0} in a few overdoped $\text{Tl}_2\text{Ba}_2\text{CuO}_{6-\delta}$ (Tl-2201) samples, and subsequently also in overdoped LSCO^{8–11}. We confirm this result for

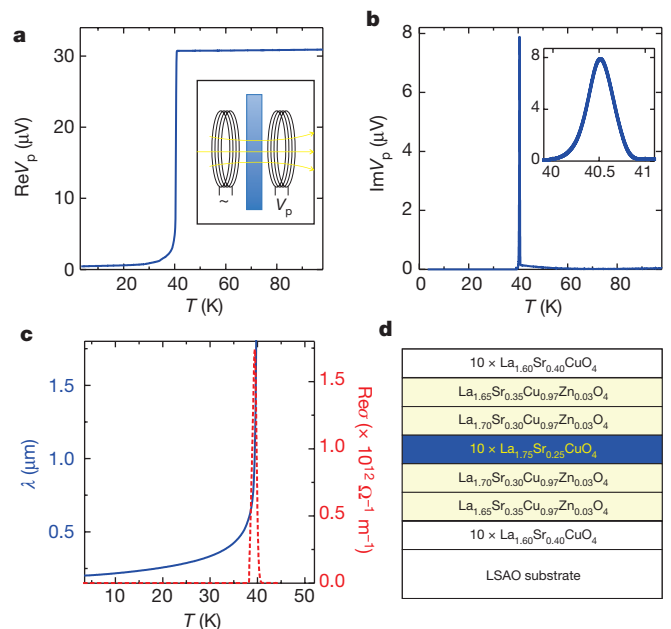


Figure 1 | Synthesis and characterization techniques. **a**, The real (in-phase) component of V_p , the voltage across the pickup coil (proportional to the mutual inductance), showing diamagnetic screening (the Meissner effect) when the film becomes superconducting. Inset, schematic of the experiment. **b**, The imaginary part of V_p shows that in this $10 \times 10 \text{ mm}^2$ film, T_c is homogeneous to better than 0.1 K. Inset, the same, near T_c . **c**, The penetration depth, λ , and the real part of the complex a.c. ($\nu = 40 \text{ kHz}$) conductivity, $\text{Re}\sigma$, derived from the complex impedance. **d**, Schematic of a sample engineered for this study at the atomic-layer level. LSAO denotes the LaSrAlO_4 substrate.

¹Brookhaven National Laboratory, Upton, New York 11973-5000, USA. ²Applied Physics Department, Yale University, New Haven, Connecticut 06520, USA.

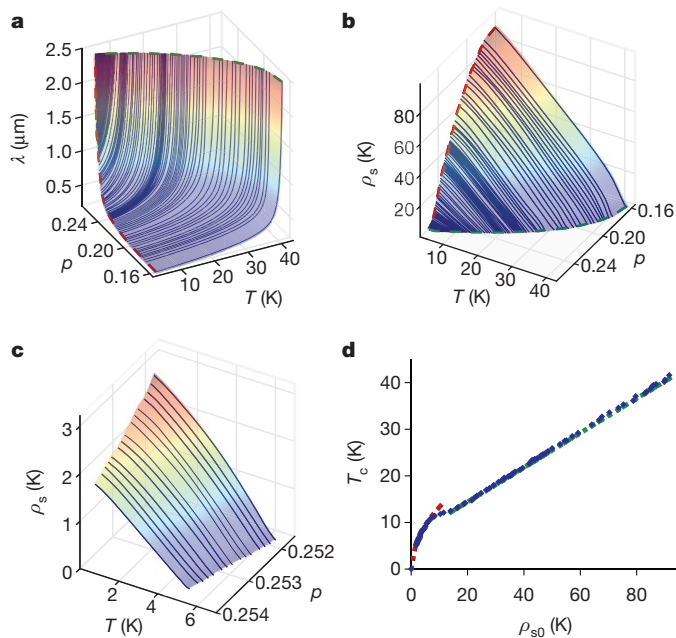


Figure 2 | The evolution of the superfluid with temperature and doping. **a**, The penetration depth $\lambda(T)$ measured in the 100 most homogeneous LSCO films synthesized by ALL-MBE. The red and green dashed lines, as well as the coloured shading, are visual aids. **b**, The corresponding phase stiffness $\rho_s(T)$. **c**, $\rho_s(T)$ for the most overdoped samples, measured down to $T = 0.3$ K. **d**, The dependence of T_c on $\rho_{s0} \equiv \rho_s(T \rightarrow 0)$. The experimental data are represented by the blue diamonds; the green dashed line is the fit to $T_c = T_0 + \alpha \rho_{s0}$ with $\alpha = 0.37 \pm 0.02$ for $\rho_{s0} > 15$ K and the red dashed line is the fit to $T_c = \gamma \sqrt{\rho_{s0}}$ with $\gamma = (4.2 \pm 0.5) \text{ K}^{1/2}$ for $\rho_{s0} < 12$ K. Source Data used to generate the lines in **b–d** are available online.

thousands of LSCO films and establish that ρ_{s0} decreases monotonously from the optimal doping until it vanishes and T_c drops to zero.

The disappearance of ρ_{s0} with overdoping was originally attributed to spontaneous electronic phase separation⁴. However, quantum oscillations observed in overdoped Tl-2201 with $T_c = 10$ K indicate electronic homogeneity on the 100 nm scale^{17,18}. We show that LSCO films grown by ALL-MBE are also intrinsically homogeneous, at every doping level.

A nearly linear $\rho_s(T)$ dependence was observed¹⁹ by a microwave technique in an overdoped Tl-2201 crystal with $T_c \approx 25$ K and very low T^{**} (2 K). We show that the same is true in LSCO films grown by ALL-MBE at every level of doping, with the slope independent of the carrier density p except very close to the edge of the dome-shaped $T_c(p)$ curve.

However, our central result, the $T_c(\rho_{s0})$ scaling law shown in Fig. 2d, differs qualitatively from these early inferences. The well-known Uemura's law, $T_c \propto n_{s0}/m^*$, inferred from muon spin rotation (μ SR) measurements⁴, refers to the underdoped side. On the overdoped side, the scarce μ SR data were interpolated by a concave 'boomerang' shape^{5–7}. In contrast, the $T_c(\rho_{s0})$ curve shown in Fig. 2d is markedly convex. The same discrepancy is found with Homes' law, $\rho_{s0} \propto \sigma_{dc} T_c$ (where σ_{dc} is the normal-state conductivity measured close to T_c), based on optics data²⁰. According to Homes' law and our measured T_c and ρ_{s0} data, $\rho_{dc} \equiv 1/\sigma_{dc}$ should increase with doping and diverge as $1/\sqrt{\rho_{s0}}$ when $\rho_{s0} \rightarrow 0$, because under these assumptions $T_c \propto \sqrt{\rho_{s0}}$ (Extended Data Fig. 8). However, our measured values of ρ_{dc} decrease monotonously (essentially linearly) with doping. These discrepancies may originate from differences in the quality and homogeneity of the samples—copper oxides are complex materials and call for advanced synthesis techniques—and in much larger error bars for the ρ_{s0} values extracted from μ SR and optics data.

A study of high-quality, heavily underdoped $\text{YBa}_2\text{Cu}_3\text{O}_{7-x}$ (YBCO) crystals by a microwave cavity-perturbation technique^{21,22} reported $\rho_s(T)$ curves that are linear down to $T^{**} \approx 4$ K. The $T_c \propto \sqrt{\rho_{s0}}$ scaling was seen over a tiny range, $0.054 < p < 0.058$ (where p is the doping

level), near the transition from superconductor to insulator and was attributed to quantum critical fluctuations. At higher doping levels, the $T_c(\rho_{s0})$ dependence became linear with a clear offset $T_0 \approx 4–5$ K. This is reminiscent of our results in Fig. 2, but in a different compound, indicating that this behaviour may be universal for the hole-doped copper oxides. Moreover, the fact that the results for underdoped YBCO are similar to those for overdoped LSCO is suggestive of underdoped/overdoped symmetry.

Our results, inferred from the raw data without any assumptions, challenge current thinking. In a clean Bardeen–Cooper–Schrieffer (BCS) superconductor, ρ_{s0} should be equal to the total particle density. (In fact, Leggett's theorem^{23,24} asserts that this is true as long as superfluidity conforms to the two-fluid scenario, and more generally for any single-species system that is translation- and time-reversal-invariant.) Pair-breaking due to impurities and disorder can reduce ρ_{s0} , but we doubt that our data can be quantitatively explained using the standard 'dirty' d -wave BCS formalism, which includes the effects of pair breaking on impurities and other defects, because in that case the Glover–Ferrell–Tinkham sum rule implies that Homes' law should apply^{20,25}, contrary to what we observe. Qualitatively, for ρ_{s0} to vanish because of disorder the sample must get extremely dirty and a superconductor-to-insulator transition would be observed, while in fact Fig. 3a shows LSCO becoming more metallic.

The $\rho_s(T)$ dependence is expected to be linear only in very clean d -wave BCS superconductors; disorder and pair-breaking turn this relation quadratic^{21,22,26} below T^{**} . In Fig. 2c, $T^{**} \lesssim 2$ K, comparable to the high-quality YBCO crystals^{21,22} and corresponding within this formalism to a mean-free-path $l_0 \gtrsim 4 \mu\text{m}$ and thus to the 'ultra-clean' limit. In Fig. 3b, we illustrate the effect of (deliberately added) disorder by comparing two samples with the same T_c (38 K), one slightly overdoped ($p = 0.19$) and clean, and the other optimally doped ($p = 0.16$) but with 0.5% of the Cu replaced by Zn, a known pair-breaker. Although this small amount of disorder does not affect T_c greatly ($\Delta T_c \approx -3$ K), it has a dramatic effect on the shape of the $\rho_s(T)$ curve, which becomes parabolic below 20–25 K. We are therefore able to detect even a small amount of disorder and pair-breaking.

The results we highlight here—the linear $\rho_s(T)$ dependence and the overall $T_c(\rho_{s0})$ scaling—are robust and not sample-dependent, and are hence likely to be intrinsic. (On the contrary, T^{**} and ρ_{dc} are affected by disorder and other extrinsic factors; both can be modified by annealing the film in a vacuum, oxygen, or ozone, thus modifying the concentration of oxygen vacancies, without a substantial effect on T_c .) The extremely dirty BCS picture is also inconsistent with observations of quantum oscillations and other experiments^{17,18,27}.

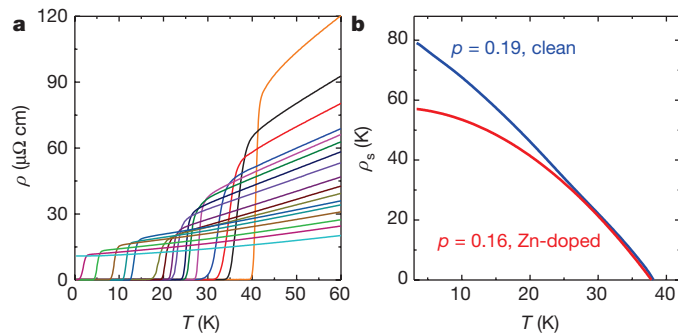


Figure 3 | Overdoped LSCO films synthesized by ALL-MBE are clean superconductors. **a**, Resistivity in LSCO films with different doping levels (see Methods), top to bottom: $p = 0.172, 0.205, 0.211, 0.217, 0.220, 0.224, 0.228, 0.230, 0.233, 0.237, 0.242, 0.245, 0.248, 0.251, 0.254, 0.258, 0.295$. **b**, The dependence of the shape of $\rho_s(T)$ on disorder. The red line represents an LSCO film that is optimally doped ($p = 0.16$) but with 0.5% of the Cu substituted by Zn. The blue line indicates a clean LSCO film that is slightly overdoped ($p = 0.19$) to have the matching T_c (approximately 38 K). In the clean film the $\rho_s(T)$ dependence is essentially linear, while in the dirty film pair-breaking makes this relation parabolic below about 25 K.

Homes' law can be derived by a different line of reasoning²⁵, assuming the 'Planckian' dissipation, with the scattering time $\tau = \hbar/k_B T$ as strong as is allowed by the uncertainty relation—which connects it naturally to another mysterious feature of HTS copper oxides, the linear temperature dependence of resistivity. The latter is probably related to the linear $\rho_{s0}(T)$ and $T_c(\rho_{s0})$ dependences we observe; as T_c and ρ_{s0} decrease with overdoping, the T -linear term in resistivity decreases as well²⁸, and this may be the reason for the deviation from the Homes relation.

Another important inference is that T_c seems to be principally controlled by the superfluid density. It seems unlikely that the doping level is the primary factor that controls both T_c and ρ_{s0} , because T_c strongly increases in LSCO under hydrostatic pressure or compressive epitaxial strain, which increases ρ_{s0} while keeping p constant²⁹. The underdoped/overdoped symmetry, even if only approximate, is another strong indication that ρ_{s0} , rather than p , controls T_c . If T_c is in fact essentially determined by the kinematics, this points to local pairing rather than to BCS physics. This notion is further supported by extensive study of the magnetoresistance in thousands of LSCO samples (I.B., J.W., A.T.B. and X.H., unpublished results), which together with the results presented here leads to the conclusion that the pair size is always smaller than their separation. However, this premise alone does not resolve the paradoxes, because Leggett's theorem^{23,24} remains valid for arbitrary interaction strengths. The fact that T_c and ρ_{s0} are comparable points to massive phase fluctuations^{11,30}, which calls any mean-field description into question. Our experimental findings therefore challenge the existing theories; the accurate scaling reported here may be a benchmark test.

Online Content Methods, along with any additional Extended Data display items and Source Data, are available in the online version of the paper; references unique to these sections appear only in the online paper.

Received 3 January; accepted 16 June 2016.

- Lee, P. A., Nagaosa, N. & Wen, X. G. Doping a Mott insulator: physics of high-temperature superconductivity. *Rev. Mod. Phys.* **78**, 17–85 (2006).
- Zaenen, J. *et al.* Towards a complete theory of high T_c . *Nat. Phys.* **2**, 138–143 (2006).
- Keimer, B., Kivelson, S. A., Norman, M. R., Uchida, S. & Zaenen, J. From quantum matter to high-temperature superconductivity in copper oxides. *Nature* **518**, 179–186 (2015).
- Uemura, Y. J. *et al.* Universal correlations between T_c and n_s/m^* (carrier density over effective mass) in high- T_c cuprate superconductors. *Phys. Rev. Lett.* **62**, 2317–2320 (1989).
- Uemura, Y. J. *et al.* Magnetic-field penetration depth in $Tl_2Ba_2CuO_{6+\delta}$ in the overdoped regime. *Nature* **364**, 605–607 (1993).
- Niedermayer, C. *et al.* Muon spin rotation study of the correlation between T_c and n_s/m^* in overdoped $Tl_2Ba_2CuO_{6+\delta}$. *Phys. Rev. Lett.* **71**, 1764–1767 (1993).
- Bernhard, C. *et al.* Magnetic penetration depth and condensate density of cuprate high- T_c superconductors determined by muon-spin-rotation experiments. *Phys. Rev. B* **52**, 10488–10498 (1995).
- Panagopoulos, C. *et al.* Superfluid response in monolayer high- T_c cuprates. *Phys. Rev. B* **67**, 220502 (2003).
- Locquet, J. P. *et al.* Variation of the in-plane penetration depth λ_{ab} as a function of doping in $La_{2-x}Sr_xCuO_{4+\delta}$ thin films on $SrTiO_3$: implications for the overdoped state. *Phys. Rev. B* **54**, 7481–7488 (1996).
- Lemberger, T. R. *et al.* Superconductor-to-metal quantum phase transition in overdoped $La_{2-x}Sr_xCuO_4$. *Phys. Rev. B* **83**, 140507 (2011).
- Rourke, P. *et al.* Phase fluctuating superconductivity in overdoped $La_{2-x}Sr_xCuO_4$. *Nat. Phys.* **7**, 455–458 (2011).
- Bozovic, I. Atomic-layer engineering of superconducting oxides: yesterday, today, tomorrow. *IEEE Trans. Appl. Supercond.* **11**, 2686–2695 (2001).
- Logvenov, G., Gozar, A. & Bozovic, I. High-temperature superconductivity in a single copper-oxygen plane. *Science* **326**, 699–702 (2009).
- Hebard, A. F. & Fiory, A. T. Evidence for the Kosterlitz–Thouless transition in thin superconducting aluminum films. *Phys. Rev. Lett.* **44**, 291–294 (1980).
- Claassen, J. H., Reeves, M. E. & Soulen, R. J. Jr. A contactless method for measurement of the critical current density and critical temperature of superconducting rings. *Rev. Sci. Instrum.* **62**, 996–1004 (1991).
- Clem, J. R. & Coffey, M. W. Vortex dynamics in a type-II superconducting film and complex linear-response functions. *Phys. Rev. B* **46**, 14662–14674 (1992).
- Vignolle, B. *et al.* Quantum oscillations in an overdoped high- T_c superconductor. *Nature* **455**, 952–955 (2008).
- Bangura, A. F. *et al.* Fermi surface and electronic homogeneity of the overdoped cuprate superconductor $Tl_2Ba_2CuO_{6+\delta}$ as revealed by quantum oscillations. *Phys. Rev. B* **82**, 140501(R) (2010).
- Deepwell, D. *et al.* Microwave conductivity and superfluid density in strongly overdoped $Tl_2Ba_2CuO_{6+\delta}$. *Phys. Rev. B* **88**, 214509 (2013).
- Homes, C. C. *et al.* A universal scaling relation in high-temperature superconductors. *Nature* **430**, 539–541 (2004).
- Hosseini, A. *et al.* Microwave spectroscopy of thermally excited quasiparticles in $YBa_2Cu_3O_{6.99}$. *Phys. Rev. B* **60**, 1349–1359 (1999).
- Broun, D. M. *et al.* Superfluid density in a highly underdoped $YBa_2Cu_3O_{6+y}$ superconductor. *Phys. Rev. Lett.* **99**, 237003 (2007).
- Leggett, A. *Quantum Liquids* Ch. 3.3–3.4 (Oxford Univ. Press, 2006).
- Leggett, A. On the superfluid fraction of an arbitrary many-body system at $T = 0$. *J. Stat. Phys.* **93**, 927–941 (1998).
- Zaenen, J. Superconductivity: why the temperature is high. *Nature* **430**, 512–513 (2004).
- Hirschfeld, P. J. & Goldenfeld, N. Effect of strong scattering on the low-temperature penetration depth of a d -wave superconductor. *Phys. Rev. B* **48**, 4219–4222 (1993).
- Allredge, J. W. *et al.* Evolution of the electronic excitation spectrum with strongly diminishing hole density in superconducting $Bi_2Sr_2CaCu_2O_{8+\delta}$. *Nat. Phys.* **4**, 319–326 (2008).
- Cooper, R. A. *et al.* Anomalous criticality in the electrical resistivity of $La_{2-x}Sr_xCuO_4$. *Science* **323**, 603–607 (2009).
- Bozovic, I., Logvenov, G., Belca, I., Narimbetov, B. & Sveklo, I. Epitaxial strain and superconductivity in $La_{2-x}Sr_xCuO_4$ thin films. *Phys. Rev. Lett.* **89**, 107001 (2002).
- Emery, V. & Kivelson, S. A. Importance of phase fluctuations in superconductors with small superfluid density. *Nature* **374**, 434–437 (1994).

Acknowledgements A. Gozar, J. Zhang and J. Yoon contributed to developing the characterization techniques during the early stages of this work. R. Sundling developed the software for the inversion of the inductance data. We also benefited from the electrolyte-gating experiments and X-ray diffraction studies by X. Leng, and from numerical simulations by N. Božović. The research was done at BNL and was supported by the US Department of Energy, Basic Energy Sciences, Materials Sciences and Engineering Division. X.H. is supported by the Gordon and Betty Moore Foundation's EPIQS Initiative through grant GBMF4410. I.B. acknowledges discussions with J. Zaenen, G. Deutscher, A. Leggett, P. Littlewood, C.-B. Eom, J. Mannhart, P. Coleman, R. Prozorov, D. van der Marel, A. McKenzie, V. Kogan, P. Armitage, J.-M. Triscone, P. Canfield, A. Chubukov, B. Halperin, P. Kim, T. Lemberger, M. V. Sadovskii, D. Pavuna, Z. Radović and M. Vanević.

Author Contributions I.B. conceived the project, synthesized the films using ALL-MBE, measured the inductance, analysed the data and wrote the text. X.H. synthesized the films, performed AFM imaging and measured the inductance. A.T.B. fabricated the devices by lithography and performed the inductance measurements in the 3He system. J.W. performed the transport measurements.

Author Information Reprints and permissions information is available at www.nature.com/reprints. The authors declare no competing financial interests. Readers are welcome to comment on the online version of the paper. Correspondence and requests for materials should be addressed to I.B. (bozovic@bnl.gov).

METHODS

Atomic-layer-by-layer molecular beam epitaxy (ALL-MBE) synthesis. In most HTS experiments so far, the main sources of uncertainty were the samples themselves. In complex materials such as copper oxides, some level of inhomogeneity is present in most samples due to extrinsic factors. Most HTS 'single crystals' in fact contain stacking faults and intergrowths of other copper oxide phases and polytypes. Moreover, oxygen is volatile in copper oxides, and hence bulk crystals are prone to gradients in the density of the oxygen vacancies or interstitials. Irregular geometries of crystals and/or contacts cause some uncertainty in transport property measurements. In principle, one can alleviate the above problems by working with very thin single-crystal films; however, most HTS films are granular and contain both secondary phase precipitates and pinholes. This calls for some advanced materials science—as well as for large sample sets with sufficient statistics to clearly discern intrinsic behaviour.

For film synthesis we use a custom ALL-MBE system¹². It is equipped with 16 metal sources (either K cells or rod-fed electron beam sources), a pure ozone source and a 16-channel real-time rate monitoring system based on atomic absorption spectroscopy. It also contains a dual-deflection reflection high-energy electron diffraction (RHEED) system that can monitor 20 samples in parallel, and a time-of-flight ion scattering and recoil spectroscopy (TOF-ISARS) system for chemical analysis of the film surface. These advanced surface science tools provide real-time information about the morphology of the film surface, the chemical composition and the crystal structure, and are also quintessential to grow atomically smooth and perfect films^{31–33}.

Using this system, we have performed over 2,500 LSCO film growth experiments. Each film was characterized in real time by RHEED and *ex situ* by atomic force microscopy (AFM) and magnetic susceptibility measurements. RHEED oscillations provide a digital count of the atomic layers and real-time control of the film quality. Selected films were also characterized *in situ* by TOF-ISARS and *ex situ* by X-ray diffraction (XRD), transport measurements and Rutherford backscattering. Further characterization was undertaken using atomic-resolution scanning transmission electron microscopy and electron energy-loss spectroscopy, resonant elastic and inelastic synchrotron X-ray scattering, synchrotron-based X-ray phase-retrieval techniques such as coherent Bragg rod analysis, muon spin rotation, ultrafast electron diffraction, ultrafast optical and THz pump-probe techniques and so on.

Using ALL-MBE, we synthesize single-crystal thin films of LSCO that are atomically smooth, without any secondary phase precipitates or pinholes. The films can be made ultrathin, down to a single unit cell thick^{31–33}; this is advantageous for transmission measurements, because a relatively large transmittance helps to minimize the effect of any small-area defects such as pinholes, which can arise from imperfections in substrate polishing, for example. Much thicker films are also grown for reflectance measurements.

To alleviate the problem of oxygen non-uniformity, we have performed over a thousand experiments that involved annealing in ozone, oxygen, or a vacuum, spanning 13 orders of magnitude in pressure from 10^{-8} torr to 200 atm. Before and after each annealing step the films were characterized by AFM, transport and XRD measurements. On the basis of these extensive studies, we have developed recipes that involve multiple annealing steps at different temperatures and pressures, yielding the most homogeneous films with the sharpest superconducting transitions.

Atomic-layer engineering. Uncertainty in the film thickness is another key problem that limits the accuracy of some measurements—of transmittance or the critical current density, for example. ALL-MBE solves this problem by providing digital control over the film thickness^{31–33}; we count atomic monolayers, while we determine the lattice constant with crystallographic accuracy by X-ray diffraction. However, this still leaves some uncertainty about the actual thickness of the superfluid, because we have found that typically a couple of layers next to the substrate are modified structurally and chemically, and are not superconducting. The same is generally true for a couple of layers near the free film surface once the film has been exposed to contamination from the atmosphere. To eliminate this problem we resort to atomic-layer engineering.

An example is illustrated in Fig. 1d. The active (superconducting) part of the sample under study is an exactly 5-unit-cell- (5-UC-) thick HTS layer. It is protected on both sides by a metallic ($M = \text{La}_{1.60}\text{Sr}_{0.40}\text{CuO}_4$) buffer and a cover layer of fixed thickness. However, without further sample engineering, there would be some hole depletion from M and accumulation in the nearest HTS layers^{31,33}. To minimize this interfacial effect, we 'sculpt' the charge profile near the interfaces by graded Sr doping in the four relevant layers. Moreover, we also dope these transition layers by substituting 3% of the Cu with Zn; this is known¹³ to suppress T_c by a factor of two and n_s even more dramatically, by four–five times. In this way, we quench any potential residual superconductivity and eliminate any interface contributions. One is then left with exactly 5 UC of superconducting material—10

HTS CuO_2 planes. We have double-checked the validity of this approach by synthesizing a series of heterostructures in which we kept the composition of the constituent materials unaltered, but varied the thickness of the active HTS layers and verified that the sheet superfluid density scaled linearly with the number of HTS CuO_2 planes (see Extended Data Fig. 1).

Note that this is just one example; indeed, we have synthesized a large number of samples, varying the layering scheme, the composition and thickness of individual layers, as well as the synthesis and post-annealing conditions. The results presented in this Letter are valid generally and not restricted to any of these choices.

Penetration depth measurements. The λ is typically measured using $\mu\text{SR}^{4-8,34}$, microwave resonance (cavity-perturbation)^{20–22,35–37}, or mutual inductance^{9,10,15–17,38–54} techniques. Because of the cost and duration, μSR experiments are usually restricted to just a few compositions and temperatures. The microwave technique offers an unsurpassed relative accuracy but the absolute accuracy is limited by the uncertainty in geometric factors. For these reasons, and because it is best suited for thin-film studies, we have chosen the mutual inductance method, which has been pioneered by several groups^{10,14,15} (Fig 1a, b). A detailed theoretical treatment¹⁶ of a superconducting film of thickness d and infinite radius, characterized by the ac conductivity $\sigma(\omega) = \sigma_1(\omega) - i\sigma_2(\omega)$, where ω is the measurement (angular) frequency and i the imaginary unit, placed between two coils of radii R_1 and R_2 , respectively, parallel to one another, and separated by a distance D , provided the following expression for the mutual inductance:

$$\begin{aligned} \hat{M} &= \text{Re}M + i\text{Im}M \\ &= \mu_0\pi R_1 R_2 \frac{\int_0^\infty dq [\exp(-qD) J_1(qR_1) J_1(qR_2)]}{\cosh(Qd) + [(Q^2 + q^2)/2qQ] \sinh(Qd)} \end{aligned} \quad (1)$$

where $\mu_0 = 4\pi \times 10^{-7}$ F m⁻¹, \mathbf{q} is the wave vector, $J_1(x)$ is the first-order Bessel function, $Q^2 = q^2 + (1/\lambda^2) - i\mu_0\omega\sigma_1$ and $\sigma_2 = 1/\mu_0\omega\lambda^2$. This is readily generalized to the case of two solenoids with N_1 and N_2 turns, respectively, by the summation over each pair of coils, one from each side. Once the values of $\text{Re}M$ and $\text{Im}M$ are measured experimentally, using equation (1) one can determine the values of λ and σ_1 .

In practice, this procedure is subject to some uncertainties because of imprecision in the coil geometry, run-to-run variations in the film position, the finite size of the film that allows some flux to 'leak' around it, other parasitic coupling between the two solenoids and inaccuracy in the film thickness. In addition, the measurements are done down to some finite temperature, most frequently $T = 4.2$ K, and the limiting value λ_0 is obtained by extrapolation. These uncertainties have been analysed in detail in the literature, and various solutions were suggested to reduce them. In what follows, we explain briefly the improvements that we made in the measuring apparatus and technique to tighten the error bars.

Parasitic field coupling around the film and through the electronics. We use inductance coils with a large number of turns (300–1,500) but very small inner radius (250 μm), much smaller than the film size (10×10 mm²), so that field leakage around the film is minimal (<0.3%) to begin with. We nevertheless subtract it accurately based on measurements of films of Nb, Pb and Al that are thick enough for transmittance to be negligible, and deposited on identical substrates. Alternatively, we deposit a thick Al overlayer on top of the HTS film and switch the diamagnetic screening in Al (at $T = 0.3$ K) between total (zero transmittance) and essentially none (total transmittance) by applying a small d.c. magnetic field (typically 100 G) that drives Al normal but does not affect the HTS film. As a consistency check, we verified that the corrected N_{s0} scales linearly with the film thickness, while being independent of frequency. (In contrast, the leakage contribution varies with frequency ν , linearly for 10 kHz $< \nu < 100$ kHz, and thus can be clearly identified by repeating measurements on the same film at several frequencies.) To minimize eddy currents, we built the sample holder out of a single block of sapphire crystal. The coils are fixed rigidly and the sample is spring-loaded so that the film surface always gets to exactly the same position. Overall, we have achieved reproducibility and precision of $\pm 0.3\%$, or better.

Uncertainty in the coil geometry. Our measured mutual inductance $M(T)$ differs a little (typically by a couple of per cent) from the calculated value due to some deviations in the geometry of the actual coil from its idealized mathematical model. To account for this (multiplicative) factor, we normalize the measured $M(T)$ by its value M_{high} just above T_c , or equivalently by M_{sub} of a pristine substrate (the latter is essentially independent of temperature and equal to M_{high}).

Field penetration through secondary phase precipitates, scratches and pinholes. This is particularly dangerous for thicker films where the intrinsic transmission is small. For this reason, we synthesize very thin films by ALL-MBE, down to 0.5 UC thick. Also, we have a very large statistics, so we can easily recognize extrinsic behaviour and factors.

Uncertainty in the film thickness. This is probably the single largest source of error^{40,45} in the measurements of λ by inductance techniques reported so far. We have minimized this using digital synthesis as described in the atomic-layer engineering section above, and illustrated in Fig. 1d. We also compared films of the same composition and T_c but of different thickness, as illustrated in Extended Data Fig. 1, and verified that the results are consistent. This constitutes the best confirmation that we can achieve at present. Regrettably, the technique described in Fig. 1d would not work on the underdoped side, but that does not affect our main goal here, which was to study the evolution of LSCO physics from the overdoped metal to the optimal doping level.

Extrapolation to $T \rightarrow 0$ of measurements done only down to $T = 4$ K. Although this has been done routinely in the literature, it may introduce error, especially for films with very low T_c —say, below about 10 K. As we are interested in behaviour near the quantum critical points where T_c vanishes, we have built a ^3He -based set-up that extends the temperature range down to 300 mK. In the same set-up, it is also possible to apply a d.c. magnetic field up to 9 T. To ensure the accuracy in temperature reading, we measure on both cooling and heating, at a very low rate of $0.1\text{--}0.2\text{ K min}^{-1}$, in a set-up where we achieve⁵⁵ a thermal stability better than 1 mK.

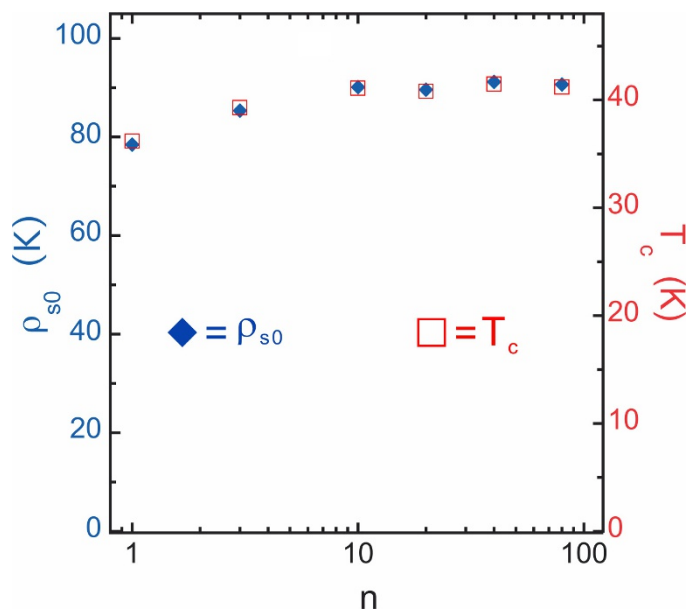
We measure $\lambda(T)$ with a reproducibility better than $\pm 0.3\%$, as illustrated for a Nb film in Extended Data Fig. 2. Altogether, the accuracy in the absolute value of λ is better than $\pm 1\%$. Moreover, some of our conclusions derive from the temperature dependence of λ , which is measured with a relative accuracy better than $\pm 0.1\%$. The same is true of ρ_s , as $\rho_s = A/\lambda^2$, and $A = \hbar^2 d/4\mu_0 k_B e^2 = 3.55 \times 10^{-12} \text{ m}^2 \text{ K}^{-1}$.

On selected films, we also compared our results with in-house high-frequency (0.5–50 MHz) inductance measurements in the reflectance geometry^{52,53}, as well as with the results of terahertz pump-probe⁵⁶ and μSR experiments³⁴ performed by our collaborators, and found good agreement.

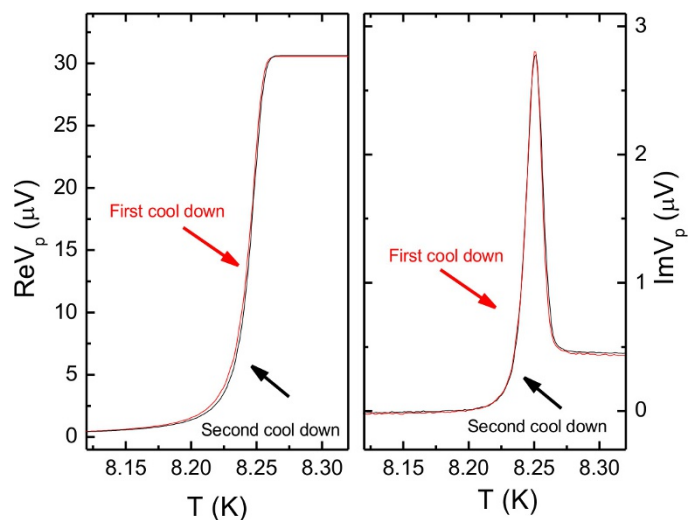
So far, we have performed inductance measurements on more than 2,500 LSCO films, a number of which were measured dozens of times and on multiple (a total of ten so far) set-ups. Mining this large database allows one to identify clear statistical trends and uncover intrinsic behaviour. In this Letter, we focus on the films with the sharpest transitions; in the best ones, near T_c we see $\sigma_1(\omega, T)$ rising exponentially on the scale of $0.1\text{--}0.2$ K. This puts an upper bound on any inhomogeneity in T_c , as the transition width comes largely from thermal fluctuations. Clearly these samples are very homogeneous and hence they can be presumed to display intrinsic properties and behaviour.

The mobile carrier density. Note that the values of p quoted here, and in the literature, are only approximately equal to the mobile carrier (hole) density. A prevailing convention in the field is to infer p from the measured T_c , assuming a parabolic $T_c(p)$ relation. This label p should roughly indicate the doping state in a particular sample. To make it easier for the reader to compare our data with various phase diagrams in the literature, in Figs 2 and 3 we provide the nominal p values inferred by assuming that in LSCO $T_c = A(p - p_{c1})(p_{c2} - p)$, with $p_{c1} = 0.06$, $p_{c2} = 0.26$ and $A = 4.15 \times 10^3 \text{ K}$, so that $p \equiv 0.16 + (0.01 - 2.4 \times 10^{-4} T_c)^{1/2}$. However, we stress that all of our conclusions are in fact only based on the quantities (T_c , λ , ρ_s and so on) that we measure directly and accurately.

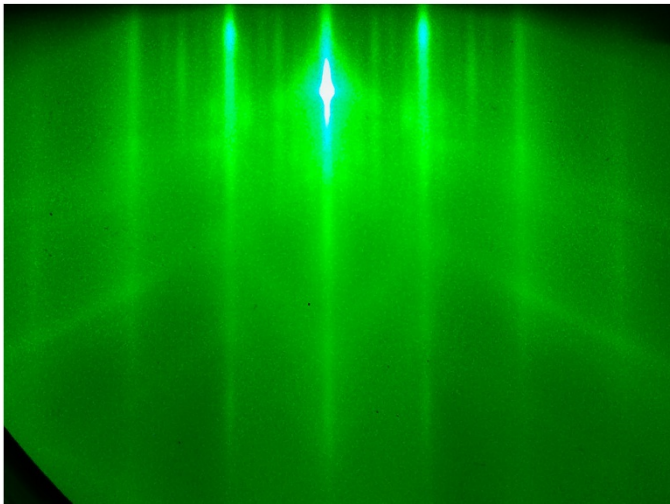
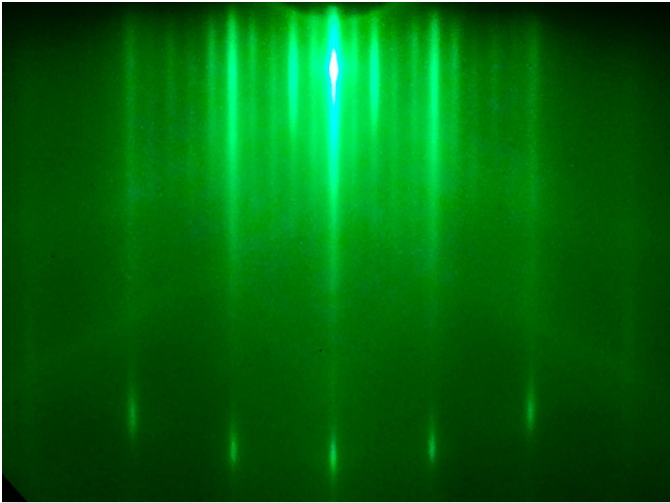
31. Gozar, A. *et al.* Interface superconductivity between a metal and a Mott insulator. *Nature* **455**, 782–785 (2008).
32. Bollinger, A. T. *et al.* Superconductor–insulator transition in $\text{La}_{2-x}\text{Sr}_x\text{CuO}_4$ at the pair quantum resistance. *Nature* **472**, 458–460 (2011).
33. Wu, J. *et al.* Anomalous independence of interface superconductivity on carrier density. *Nat. Mater.* **12**, 877–881 (2013).
34. Morenzoni, E. *et al.* The Meissner effect in a strongly underdoped cuprate above its critical temperature. *Nat. Commun.* **2**, 272 (2010).
35. Bonn, D. A. & Hardy, W. N. in *Physical Properties of High Temperature Superconductors* Vol. V (ed. Ginsberg, D. M.) 7–98 (World Scientific, 1996).
36. Prozorov, R. & Giannetta, R. W. Magnetic penetration depth in unconventional superconductors. *Supercond. Sci. Technol.* **19**, R41–R67 (2006).
37. Prozorov, R. & Kogan, V. G. London penetration depth in iron-based superconductors. *Rep. Prog. Phys.* **74**, 124505 (2011).
38. Lee, J. Y. & Lemberger, T. R. Penetration depth $\lambda(T)$ of $\text{YBa}_2\text{Cu}_3\text{O}_{7-\delta}$ films determined from the kinetic inductance. *Appl. Phys. Lett.* **62**, 2419–2421 (1993).
39. Pippard, A. B. Magnetic penetration depth through a superconducting film. *Supercond. Sci. Technol.* **7**, 696–699 (1994).
40. Turneure, S. J., Ulm, E. R. & Lemberger, T. R. Numerical modeling of a two-coil apparatus for measuring the magnetic penetration depth in superconducting films and arrays. *J. Appl. Phys.* **79**, 4221–4227 (1996).
41. Fuchs, A., Prusseit, W., Berberich, P. & Kinder, H. High-precision penetration-depth measurement of $\text{YBa}_2\text{Cu}_3\text{O}_{7-\delta}$ as a function of oxygen content. *Phys. Rev. B* **53**, R14745–R14748 (1996).
42. Gilchrist, J. & Brandt, E. H. Screening effect of Ohmic and superconducting planar thin films. *Phys. Rev. B* **54**, 3530–3544 (1996).
43. Lee, J. Y., Kim, Y. H., Hahn, T.-S. & Choi, S. S. Determining the absolute value of penetration depth of large area films. *Appl. Phys. Lett.* **69**, 1637–1639 (1996).
44. Claassen, J. H., Wilson, M. L., Byers, J. M. & Adrian, S. Optimizing the two-coil mutual inductance measurement of the superconducting penetration depth in thin films. *J. Appl. Phys.* **82**, 3028–3034 (1997).
45. Turneure, S. J., Pesetski, A. A. & Lemberger, T. R. Numerical modeling and experimental considerations for a two-coil apparatus to measure the complex conductivity of superconducting films. *J. Appl. Phys.* **83**, 4334–4343 (1998).
46. Paget, K. M. *et al.* Magnetic penetration depth in superconducting $\text{La}_{2-x}\text{Sr}_x\text{CuO}_4$ films. *Phys. Rev. B* **59**, 641–646 (1999).
47. Wang, R. F., Zhao, S. P., Chen, G. H. & Yang, Q. S. Absolute measurement of penetration depth in a superconducting film by the two-coil technique. *Appl. Phys. Lett.* **75**, 3865–3867 (1999).
48. Coffey, M. W. Analyzing mutual inductance measurements to determine the London penetration depth. *J. Appl. Phys.* **87**, 4344–4351 (2000).
49. Coffey, M. W. Mutual inductance of superconducting thin films. *J. Appl. Phys.* **89**, 5570–5577 (2001).
50. Rufenacht, A., Locquet, J. P., Fompeyrine, J., Caimi, D. & Martinoli, P. Electrostatic modulation of the superfluid density in an ultrathin $\text{La}_{2-x}\text{Sr}_x\text{CuO}_4$ film. *Phys. Rev. Lett.* **96**, 227002 (2006).
51. Lemberger, T. R., Hetel, I., Tsukada, A. & Naito, M. Anomalous sharp superconducting transitions in overdoped $\text{La}_{2-x}\text{Sr}_x\text{CuO}_4$ films. *Phys. Rev. B* **82**, 214513 (2010).
52. Gauzzi, A. *et al.* Very high resolution measurement of the penetration depth of superconductors by a novel single-coil inductance technique. *Rev. Sci. Instrum.* **71**, 2147–2153 (2000).
53. Gasparov, V. A. & Bozovic, I. Magnetic field and temperature dependence of complex conductance of ultrathin $\text{La}_{1.55}\text{Sr}_{0.45}\text{CuO}_4/\text{La}_2\text{CuO}_4$ films. *Phys. Rev. B* **86**, 094523 (2012).
54. Došlić, M., Pelc, D. & Požek, M. Contactless measurement of nonlinear conductivity in the radio-frequency range. *Rev. Sci. Instrum.* **85**, 073905 (2014).
55. Dubuis, G., He, X. & Božović, I. Ultra-thermal-stabilization of a closed cycle cryocooler. *Rev. Sci. Instrum.* **85**, 103902 (2014).
56. Bilbro, L. S. *et al.* Temporal correlations of superconductivity above the transition temperature in $\text{La}_{2-x}\text{Sr}_x\text{CuO}_4$ probed by terahertz spectroscopy. *Nat. Phys.* **7**, 298–302 (2011).
57. Donnelly, R. J. in *Physics Vade Mecum* (ed. Anderson, H. L.) 121, Table E (AIP New York 1981).
58. Homes, C. C., Dordevic, S. V., Bonn, D. A., Liang, R. & Hardy, W. N. Sum rules and energy scales in the high-temperature superconductor $\text{YBa}_2\text{Cu}_3\text{O}_{6+x}$. *Phys. Rev. B* **69**, 024514 (2004).
59. Homes, C. C., Dordevic, S. V., Valla, T. & Strongin, M. Scaling of the superfluid density in high-temperature superconductors. *Phys. Rev. B* **72**, 134517 (2005).
60. Tallon, J. L., Cooper, J. R., Naqib, S. H. & Loram, J. W. Scaling relation for the superfluid density of cuprate superconductors: origins and limits. *Phys. Rev. B* **73**, 180504(R) (2006).



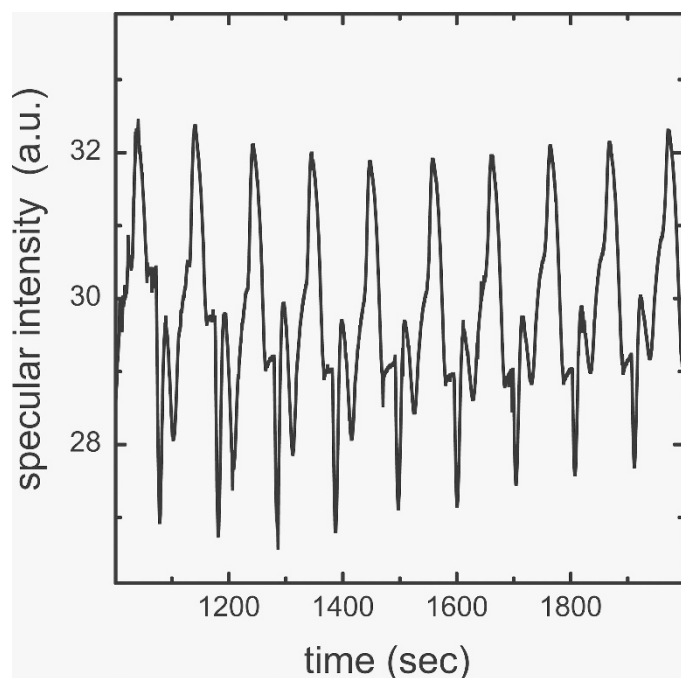
Extended Data Figure 1 | The dependence of T_c on ρ_{s0} in several LSCO films. The films have the same nominal doping near the optimal ($p = 0.16$) in the active (superconducting) layer, but with different thickness $D = nd$, where $d = 0.662$ nm and $n = 1, 2, 4, 10, 40$ and 80 . Although individually both T_c and ρ_{s0} show some random variations, in part due to imperfect control of the doping level and the density of the oxygen vacancies, their ratio apparently stays almost constant, to about $\pm 1\%$. This reinforces the conclusion that T_c is indeed essentially controlled by ρ_{s0} , a purely kinematic quantity.



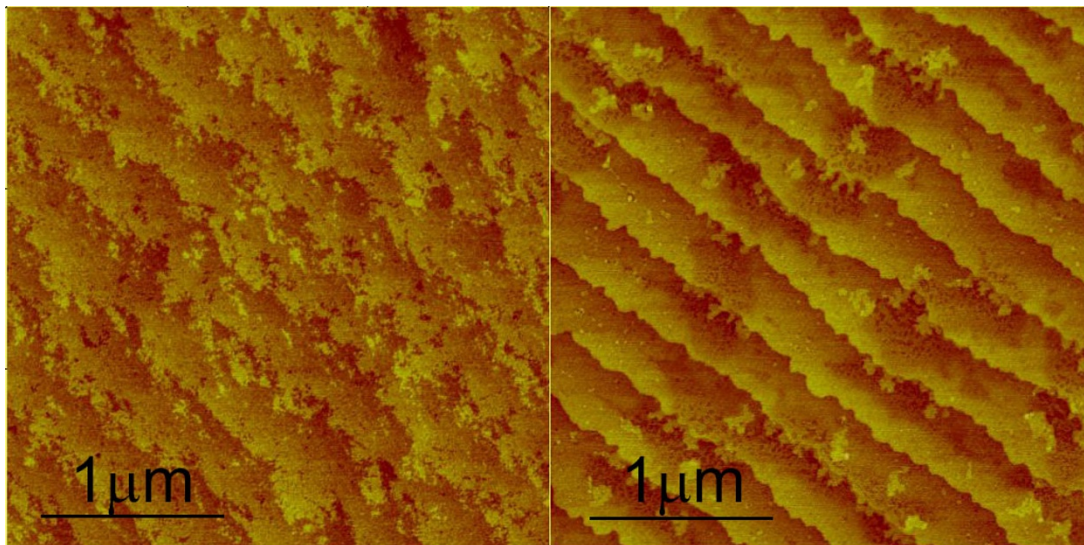
Extended Data Figure 2 | Mutual inductance (raw data) measured on a (275 ± 12) -nm-thick Nb film deposited on standard $10 \times 10 \times 1$ mm³ LaSrAlO₄ substrates. The film was measured on 22 March 2015 (red lines) and 20 January 2016 (black lines). The thermal stabilization is better than ± 1 mK and the overall reproducibility is better than $\pm 0.3\%$ on a one-year scale. The inferred value of $\lambda_0 = (41 \pm 5)$ nm agrees with values in the literature⁵⁷; the error here largely comes from the uncertainty in the film thickness. This error is much smaller (down to less than $\pm 1\%$) in the case of our LSCO films, where we employ atomic-layer deposition, which provides digital control of the film thickness.



Extended Data Figure 3 | RHEED recorded during growth of LSCO films by ALL-MBE. Top, an optimally doped ($p = 0.16$, $T_c = 40$ K) LSCO film after the end of growth process. Bottom, a strongly overdoped LSCO film ($p = 0.24$, $T_c = 7.5$ K). The stronger main streaks correspond to Bragg-rod reflections at very shallow angles from a terraced surface. The four weaker sidebands in between every pair of main streaks indicate a ubiquitous $5a_0 \times 5a_0$ surface reconstruction (where $a_0 = 0.38$ nm is the in-plane lattice constant). The diagonal streaks are so-called Kikuchi lines that are formed by inelastically scattered electrons; they are observable only from atomically perfect surfaces.



Extended Data Figure 4 | RHEED oscillations recorded during the growth of an LSCO film by ALL-MBE. In the atomic-layer growth mode, the intensity of the specular beam oscillates. When 2D islands form on the surface, the diffuse reflectance increases as the specular reflectance decreases, until about half of the surface is covered. Then the specular reflectance increases again, reaching a new maximum at the full coverage. The fact that the amplitude of the oscillations does not decrease indicates perfect atomic-layer growth. The number of periods provides digital information on the film thickness, expressed in the units of the lattice constant (which we know accurately from XRD).

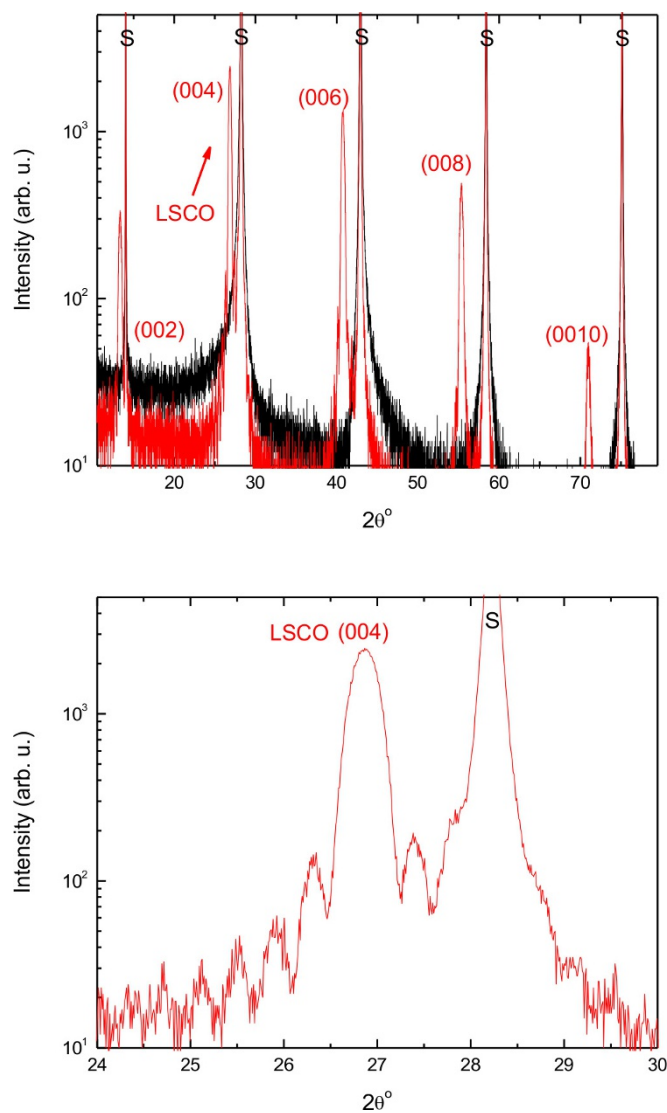


LSAO substrate
rms roughness:0.205nm

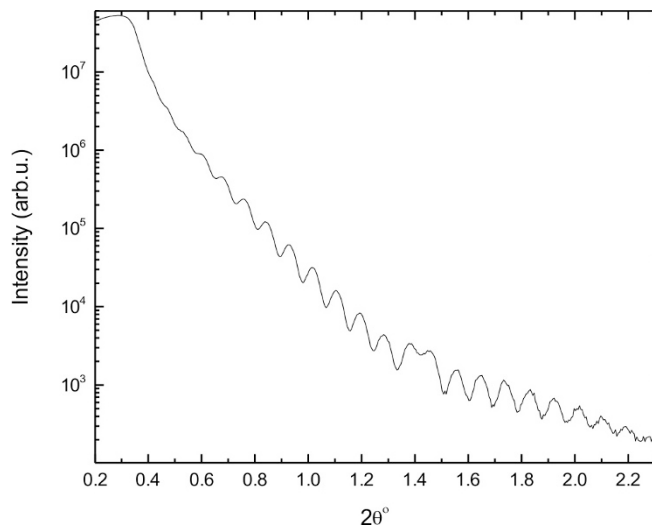
LSCO film
rms roughness:0.239nm

Extended Data Figure 5 | AFM images showing the quality of the film surfaces. Left, an LSAO substrate. The steps, 0.5 UC (0.65 nm) high, occur because the polished surface is unintentionally (but unavoidably) oriented slightly (typically by less than 0.3°) off the desired crystallographic plane perpendicular to the [001] direction. Right, a 225-Å-thick LSCO film

grown on the same substrate. The steps in the substrate are projected onto the film and persist all the way to the film surface, indicating atomic-layer growth. The overall root-mean-square (r.m.s.) surface roughness is about 0.24 nm; the terraces between steps are atomically smooth.



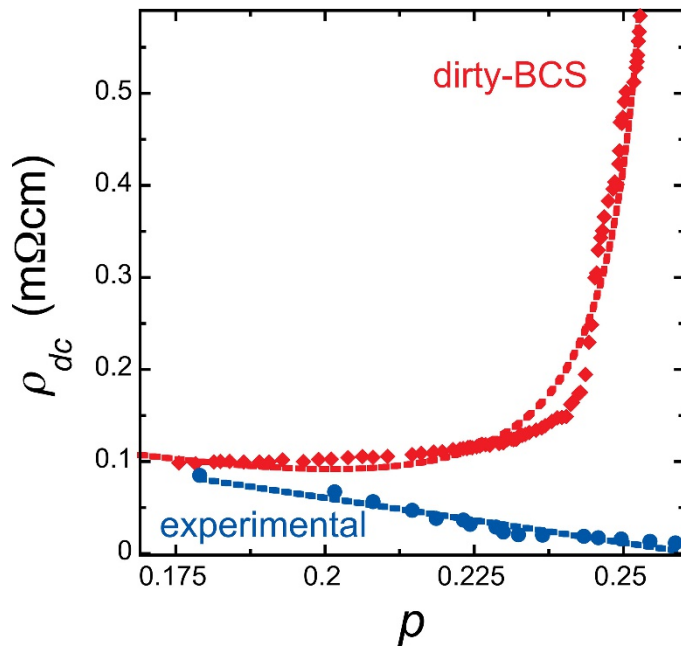
Extended Data Figure 6 | A wide-angle 2θ XRD pattern of an LSCO film grown on an LSAO substrate by ALL-MBE. The top panel shows a pristine LSAO substrate (black) and an LSCO film grown on the same substrate (red). Only even-order reflections are allowed by the space-group symmetry. The substrate peaks are labelled S. There are no traces of any other phases. The bottom panel is an expanded view near the (004) LSCO reflection. The side-bands between the LSCO Bragg reflections are the so-called Laue (or finite-thickness) fringes that originate from the interference between X-rays reflected from the film surface and the substrate–film interface.



Extended Data Figure 7 | Low-angle X-ray reflectivity measured from an LSCO film grown on an LSAO substrate by ALL-MBE.

The oscillations are so-called Kiesig fringes that originate from interference between X-rays reflected from the film surface and the substrate–film interface. They are analogous to a Fabry–Perot interferogram, and indicate that the two ‘mirrors’ are smooth and parallel on the scale of the wavelength of light (here, 1.54 Å).

By comparing with simulated interferograms, one can estimate the film thickness and roughness; the estimates agree well with the thickness inferred from the digital count of the unit cells by RHEED and the surface roughness as determined by AFM.



Extended Data Figure 8 | Failure of the dirty BCS model to account for experimental data. The red diamonds represent ρ_{dc} calculated from our measured T_c and ρ_{s0} values by applying Homes' law, $\rho_{s0} \propto \sigma_{dc} T_c$, which follows from the Ferrell–Glover–Tinkham sum rule for dirty BCS superconductors^{23,28,58–60}. As $T_c \propto \sqrt{\rho_{s0}}$ at high overdoping, the predicted ρ_{dc} value diverges as $1/\sqrt{\rho_{s0}}$, which should trigger a superconductor-to-insulator transition. The red dashed line is a fit to $f(p) = c_1 + c_2 p + c_3 / (0.26 - p)$. Blue circles are the measured ρ_{dc} values (from the data shown in Fig. 3a) showing that the samples in fact get more metallic. The blue dashed line is a fit to $f(p) = c_1 - c_2 p$. The gross discrepancy with the experiment implies that the original premise—the dirty BCS scenario—is incorrect.